EXPERIMENTAL AND NUMERICAL STUDIES ON A CENTRIFUGAL PUMP WITH 2D-CURVED BLADES IN CAVITATING CONDITION

M. HOFMANN, B. STOFFEL
Laboratory for Turbomachinery and Fluid Power, Darmstadt University of Technology, Germany

O. COUTIER-DELGOSHA, R. FORTES-PATELLA, JL. REBOUD(*)
Laboratoire des Ecoulements Géophysiques et Industriels, Grenoble, France
(*) LTDS/ENISE, Saint Etienne, France

Abstract
In the presented study a special test-pump with 2D curvature blade geometry in cavitating and non-cavitating conditions was investigated using different experimental techniques and a 3D numerical model of cavitating flows. Experimental and numerical results concerning pump characteristics and performance breakdown were compared at different flow conditions. Appearing types of cavitation and the spatial distribution of vapour structures within the runner were also analysed.

1. Introduction
In the scope of the European Research Program PROCOPE, researchers of the TUD (Laboratory for Turbomachinery and Fluid Power at Darmstadt) and of the LEGI (Laboratoire des Ecoulements Géophysiques et Industriels de Grenoble) work together in order to improve the understanding of the unsteady behaviour of cavitating flows and the related erosive aggressiveness.
In order to extend previous analyses concerning the cavitating flows around a 2D-hydrofoil [Hofmann et al., 1999] and in a cascade of three hydrofoils [Lohrberg et al., 2001], the present study consists of investigations by experimental means and numerical simulation concerning a special centrifugal test-pump in cavitating and non-cavitating conditions. Experiments were carried out at Darmstadt University of Technology using different experimental techniques. The measurement of classical pump characteristics and performance breakdown at different flow conditions were associated with flows visualisations. Appearing types of cavitation and the spatial distribution of vapour structures within the runner were analysed.
Three-dimensional Navier-Stokes codes taking into account the cavitation process have been developed during the last years [Takasugi et al., 1993, Alajbegovic et al., 1999, Kunz et al., 1999, Bunnel and Heister, 2000] based on different multi-phase flow approaches [Delannoy and Kueny, 1990, Kubota et al. 1992]. Industrial CFD codes are now starting to take into account cavitation models, allowing first applications to pump geometries [Combes and Archer, 2000]. In this context, a numerical model for three-dimensional cavitating flows is developed at LEGI, based on the 3D code FINE/TURBO^{TM}, developed by NUMECA International. That work is performed in cooperation with SNECMA Moteurs and the French space agency CNES, with the final objective to provide accurate simulations of unsteady cavitating flows in the inducers of rocket engine turbo-pumps [Coutier-Delgosha et al. 2001a,b]. The application to the centrifugal pump represents a first step of validation of the model on steady-state cavitating flow in turbomachinery.

2. Geometry
A special runner geometry has been chosen to easily adapt existing measuring techniques for a single hydrofoil in a test section [Hofmann et al., 1999, Hofmann, 2001] to a pump test-rig. Optical access in 2 planes was made possible to enable a view perpendicular to the blade surface on both suction and pressure side by Plexiglas windows in the housing and a Plexiglas shroud. The runner has 5 single-curved blades with two different radii at inlet and outlet. The part of the blade with the larger radius (the second part in flow direction) was also made of Plexiglas to obtain optical access to the pressure side of the following blade and the entire channel respectively.
Figure 1a shows the intersection of the 2 blade radii. Another characteristic is the parallel hub and shroud to get an almost 2-dimensional blade-to-blade channel with constant width.
A radial-symmetric housing (Figure 1b) is used to obtain almost constant conditions on the runner outlet (if we neglect gravitational forces which are small compared to the performance of the runner). With these preconditions we obtain comparable cavitation conditions in each channel without the influence of a volute casing.

Nominal conditions are at a rotational speed of 36 Hz and a flow-rate q = 210 m^3/h. Specific speed of the runner is $n_s = n\ Q^{1/2} / H^{3/4} = 20$ (europ. value: n in rpm, Q in m^3/s and H in m), the outer runner diameter equals 278 mm. Cavitation conditions are defined by NPSH value based on the upstream total pressure, water vapour pressure and density at ambient temperature.

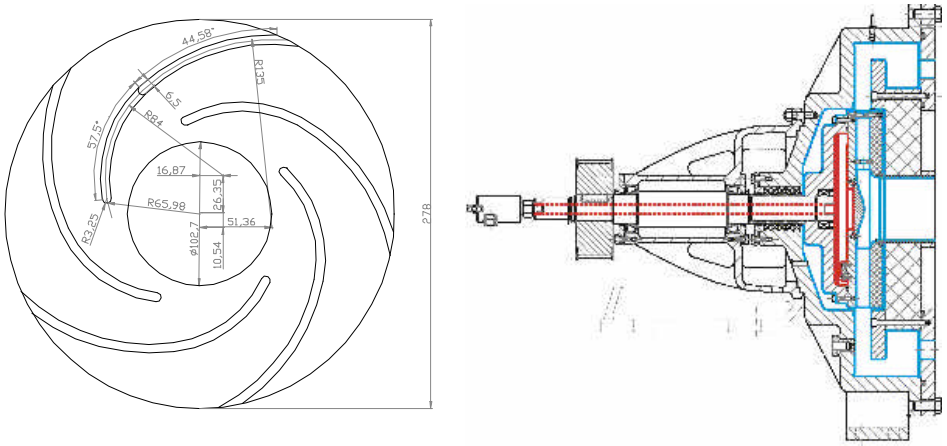

Figure 1a. runner geometry ; 1b. housing

3. Visualisations

Besides the measurements of the characteristics of the pump at different flow-rates and cavitation conditions, various visualisation techniques were used. All images shown in this paper were done at nominal flow rate with various values of NPSH, where both cavitation on suction and pressure side of the blades occurs.

Stroboscopic light was used on one hand for standard imaging and High-Speed-Video with the Light-Sheet-Illumination (Figure 2) was applied to observe self-oscillating states of the cavitation on the blade pressure side or other unsteady effects [Hofmann et al., 2001].

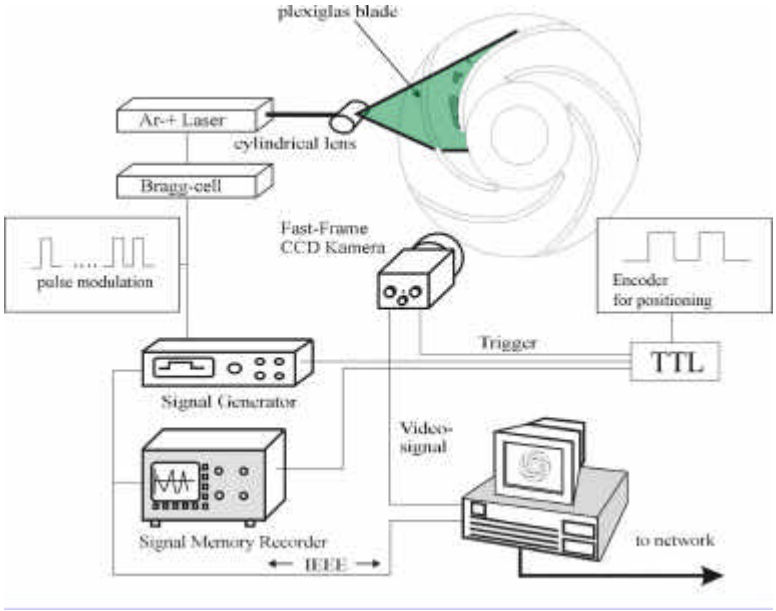

Figure 2. Visualisation set-up

The investigated flow conditions during the experiments show always unsteady behaviour of the leading edge cavitation, not only concerning the unsteadiness of the closure region of the attached cavitation but also the shedding of vapour structures in the channel. Besides the well known attached cavitation on pressure and suction side, another type of cavitation occurs on the inlet of the runner caused by the strong curvature of the streamlines. It is visible

either as attached cavitation caused by the depression at the radius (regions B and C in Figure 3), or as shear cavitation because the flow was separating at the inlet radius of the shroud at lower values of NPSH (region B in figure 4). Dependent on the length of the attached part of the cavitation (region A in all figures) the extent of this shear layer cavitation leads into the channel as it is shown in Figure 4 at two different stages of a cavitation cycle. In Figure 4a the larger extent of the shear cavitation (region B) on top of the attached part (see region A, the illuminated interface of the cavitation sheet on pressure side) is visible. In Figure 4b (with a smaller cavitation sheet) no shear cavitation can be seen. The contour of the interface of the attached part of the cavitation (region A) already indicates a different state of the typical self oscillating cloud cavitation condition.

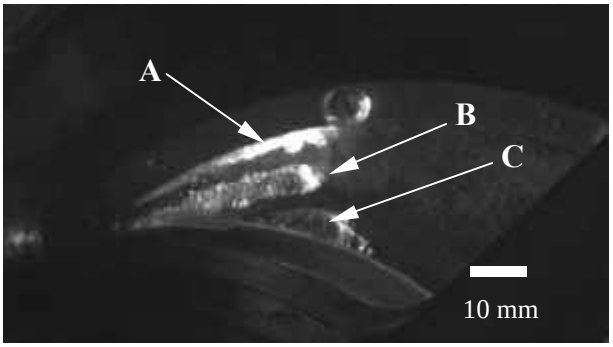

Figure 3. Unsteady state of blade cavitation on suction side, NPSH = 8m. (stroboscopic light illumination)
(A scaling bar is added to each image, representing a length of 10 mm)

With the aid of Laser-Light-Sheet-Illumination of the vapour-fluid-interface, an analysis of the unsteadiness of the attached part of the cavitation in the runner could be done in the middle of the channel. The images were taken with a rate of 2 Hz but triggered by an angular decoder within the motor and a special conditioning which allowed to take the image at every phase angle compared to a reference angle with a step size of 1 degree. Hence, the illuminated blade had 18 revolutions between every image.

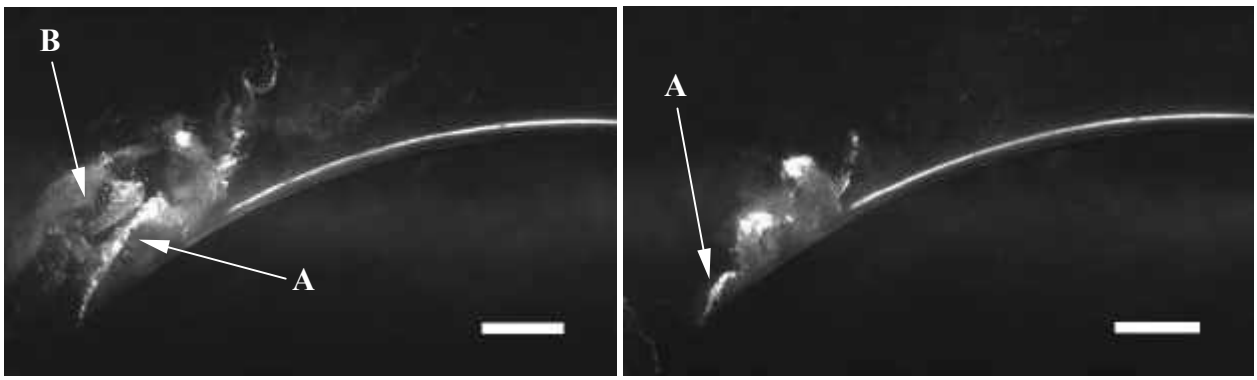

Fig. 4: unsteady state of blade cavitation on pressure side at two different time and NPSH = 7 m (Laser light sheet)

Based on 500 images, illuminated with 50 µs, a mean grey value distribution was calculated to identify the mean cavity on the leading edge of the blade.
The standard deviation of the grey values or its variance can serve as a value for the unsteadiness of the cavitation. In regions of the image with higher values of the variance, the fluctuations of the grey values, and therefore the fluctuations of the reflecting vapour structures, are larger than in regions with a smaller variance. Those regions are constantly filled with either water or vapour. The result of such a treatment is shown in Figures 5 and 6.
Mean distribution (Figure 5a and 6a): The attached part of the cavitation can only be identified by its 2-phase-interface, because the light sheet is mainly reflected. But the mean region with a cloud shedding is also indicated by a higher mean grey value just after the closure region of the cavitation sheet. For the numerical comparison we just identify the attached part. As expected, the extent of both regions enlarges with decreasing NPSH-value. As already mentioned, the flow has the tendency to separate on the leading edge of the blade, which is supported (Figure 6a) at lower pressure conditions.

Standard deviation (Figure 5b and 6b): The fluctuation of the shedding becomes larger with decreasing NPSH and its extension fills almost half of the height of the channel. This is a result of the higher production of transient vapour structures from the leading edge cavitation. The interface of the attached cavitation seems in contrast to be rather stable. Probably the flow is clearly separated from the leading edge, the separation zone fills almost steady with vapour, and only in the closure region vapour is shed into the channel.

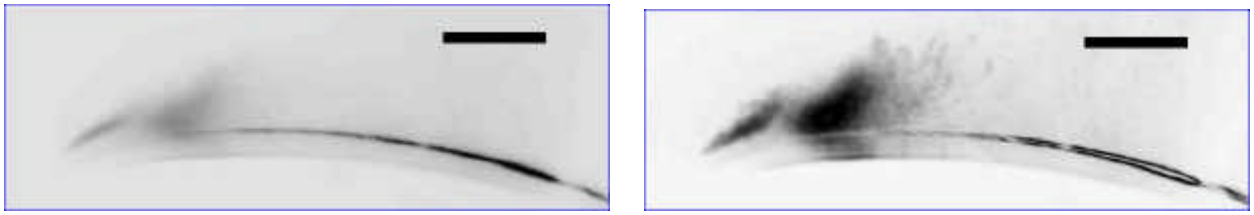

Figure 5. Mean vapour distribution and standard deviation Qn , NPSH = 7 m

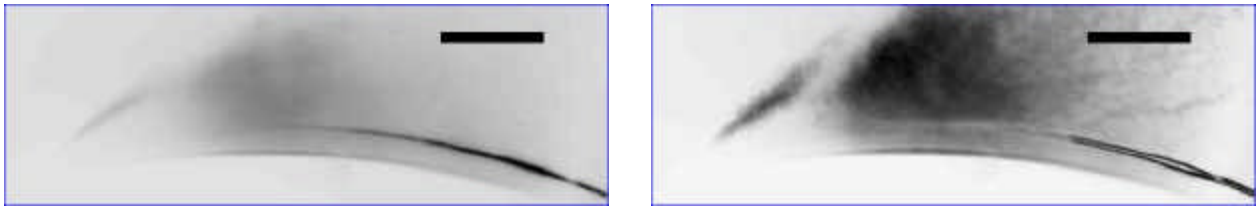

Figure 6. Mean vapour distribution and standard deviation Qn , NPSH = 6 m

4. Physical and numerical model

The mean features of the physical and numerical models are summarized in the present paper. More details are given in [Coutier-Delgosha et al., 2001b].

Cavitating flows are described by a single fluid model, based on previous numerical and physical work developed in LEGI [Delannoy and Kueny, 1990, Reboud et al. 1998]. This fluid is characterised by a density ρ that varies in the computational domain: when the density in a cell equals the liquid one (ρ_l), the whole cell is occupied by liquid, and if it equals the vapour one (ρ_v), the cell is full of vapour. Between these two extreme values, a liquid/vapour mixture, still considered as one single fluid, occupies the cell. The void fraction $\alpha = (\rho - \rho_l) / (\rho_v - \rho_l)$ can thus be defined as the local ratio of vapour contained in this homogeneous mixture.

Velocities are assumed to be locally the same for liquid and for vapour. An empirical state law is used to manage the mass fluxes resulting from vaporisation and condensation processes. That barotropic law links the density to the local static pressure $\rho(P)$. When the pressure is higher or lower than vapour pressure, the fluid is supposed to be purely liquid or purely vapour, according to the Tait equation or to the perfect gas law respectively. The two fluid states are joined smoothly in the vapour-pressure neighbourhood. It results in the evolution law presented in Figure 7, characterized mainly by its maximum slope $1/A_{min}^2$, where $A_{min}^2 = \partial P/\partial \rho$. A_{min} can thus be interpreted as the minimum speed of sound in the mixture.

The numerical model of cavitating flows based on that physical description is developed from the commercial code FINE/TURBO^{TM} developed by NUMECA International. FINE/TURBO^{TM} is a three-dimensional structured mesh code that solves the time dependant Reynolds-Averaged Navier-Stokes equations. Time accurate resolutions of the equations use the dual time stepping approach. Pseudo-time derivative terms are added to march the solution towards convergence at each physical time step. The range of application is extended to low-compressible or incompressible flows by introducing a preconditioning matrix [Hakimi, 1997].

The discretization is based on a finite volume approach. Convection terms are treated by a second order central scheme associated with artificial dissipation terms. The pseudo-time integration is made by a four-step Runge-Kutta procedure. The physical time-derivative terms are discretized with a second order backward difference scheme.

The code resorts to a multigrid strategy to accelerate the convergence, associated with a local time stepping and an implicit residual smoothing.

The numerical model was adapted to treat the cavitation process [Coutier-Delgosha et al., 2001a]. The key point of this adaptation is the modification of the state law of the fluid. Applied barotropic law implies the simultaneous treatment of two different cases: the fluid is highly compressible in the liquid/vapour mixture (the Mach number can be as high as 4 or 5) and is almost incompressible in the pure vapour or pure liquid areas. So the main difficulty consisted in managing these two different states of the fluid, without creating any spurious discontinuity in the flow

field. Besides, cavitation consists in a very sharp and very rapid process. The density variations in time and space are smoothed to avoid numerical instabilities.

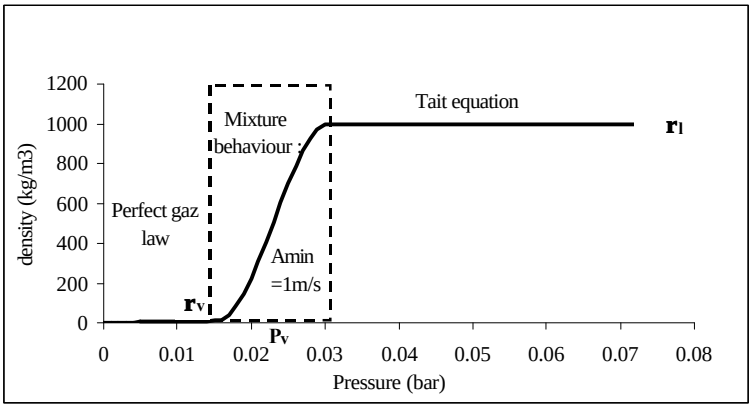

Figure 7: The barotropic state law ρ(P) for water.

The model was applied to the presented centrifugal pump geometry. 300.000 cells multi-blocks mesh of one single blade-to-blade channel was used (Figure 8). Conditions applied for the simulations are the following:

- Turbulence model: we use for the simulations presented in this paper a Baldwin-Lomax turbulence model.
- Boundary conditions: Velocity is imposed at the inlet of the suction pipe. Laws of the wall are imposed along solid boundaries. The relative motion between the inlet pipe walls and the runner is taken into account. On the other hand, the outlet housing shape is not described and the parallel walls are treated as hub and shroud extensions up to the outlet, at 1.5 times the runner outer radius, where a uniform static pressure is imposed.
- Initial transient treatment: First of all, a steady step is carried out, with a pseudo vapour pressure low enough to ensure non cavitating conditions in the whole computational domain. Then, the NPSH is slowly lowered by increasing smoothly the pseudo vapour pressure at each new time step up to the physical value. Vapour structures spontaneously appear and grow during that process, in the regions of low static pressure. The final NPSH value, depending on the outlet static pressure imposed, is then kept constant throughout the computation.

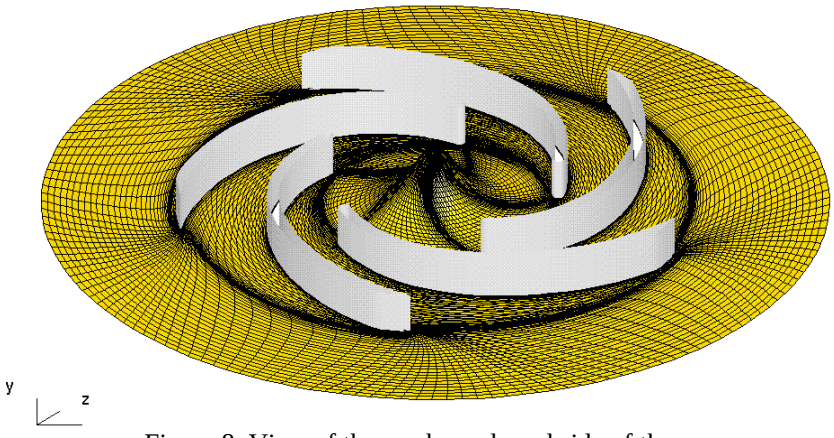

Figure 8. View of the mesh on shroud side of the pump.
(the entire pump geometry is reconstructed by rotation of the single blade-to-blade channel)

5. Non-cavitating characteristics

Experimental tests and numerical calculations were performed considering a large range of flow-rates, in non-cavitating conditions. Figure 9a illustrates the computational result at nominal flow rate: the total pressure elevation is represented in the middle of the pump channels. Figure 9b presents a comparison between the numerical and experimental performance charts. Directly based on the measurements performed, the head of the pump is defined as the difference between downstream static pressure and upstream total pressure.

We observe a reliable agreement between the pump characteristics given by measurement and computation in the whole range of flow rates investigated experimentally. The model gives a better prediction when the flow rate is over

50% of the nominal value (Qn = 210m^3/h), and the numerical simulation becomes unstable at very low partial flow rate. As a matter of fact, the numerical simulation slightly overestimates the pump head. This is an expected result, since the flow through the side chamber is not taken into account in numerical simulations. This gap flow of the pump impeller has to be added to the flow rate actually passing through the blade-to-blade channels and is therefore slightly higher in the experiments than in the model. At nominal flow rate, the head is overestimated of about 5% (40.5m instead of 38.5m). The uncertainty on the measured value was estimated to max. 80 cm and corresponds to 2% of the value, which also has to be taken into account.

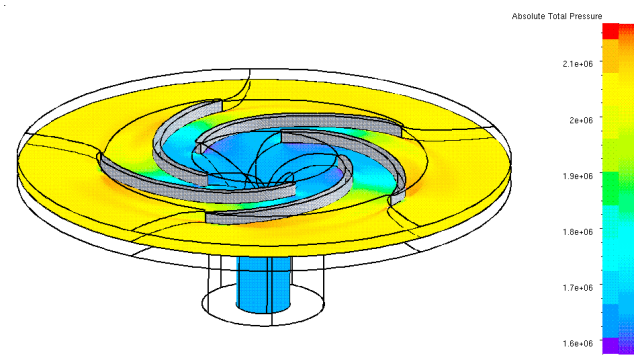

Figure 9a. Total pressure field in the pump (nominal flow rate)

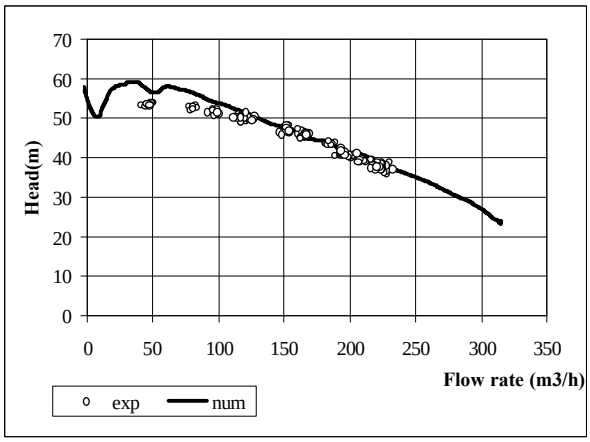

9b.Characteristics H(Q) of the pump

7. Cavitation behaviour

Numerical simulation of the cavitation characteristics of the pump was performed at different flow rates. The shape of the cavitating structures is first compared to the experimental visualisations presented above at nominal flow rate. When the NPSH decreases in the calculation, attached cavitation sheets grow both on the suction side and on the pressure side, as observed experimentally. Moreover, vapour structures appear at the inlet radius of the shroud. This cavitation caused by the local curvature of the streamlines is fully consistent with the observations reported previously. The visualisation obtained in Figure 3 is applied to the computational result to enhance the reliable agreement. The cavitation number was adjusted to give the same global extent of the cavitation structures than in the experiment: the numerical result then corresponds to a NPSH about 10% lower than the experimental one (7 m, instead of 8 m). The three cavitation areas are correctly simulated by the code (Figure 10): attached cavity on the suction side (A), extent of cavitation on the shroud along the blade (B), and cavitating flow on the inlet radius of the shroud (C). In the computation, attached sheet cavity (A) and extent on the shroud (B) belong to the same vapour structure, while they look like two separated regions in the experiment.

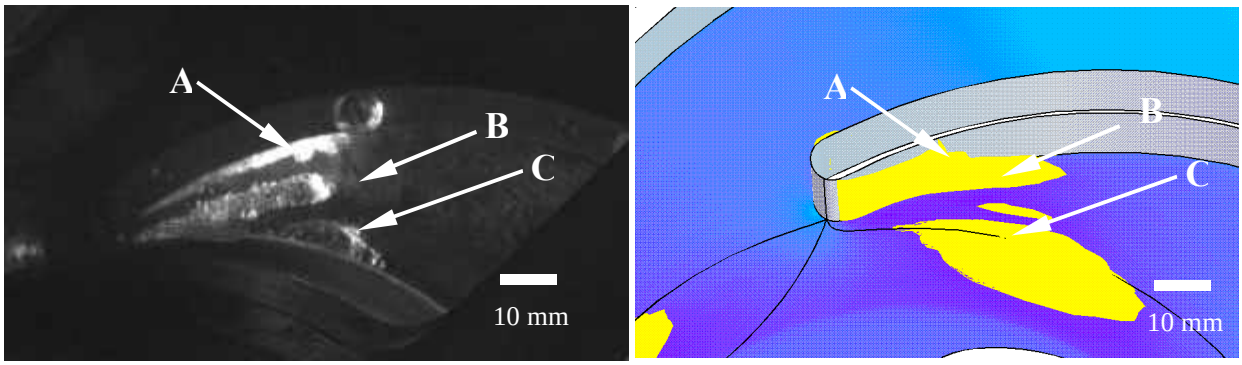

Figure 10. Vapour structures on suction side (experiment NPSH=8m, computation NPSH = 7m).
Calculation: iso-density contour ($\rho \approx 0.95\rho_l$: void ratio >5%) drawn in yellow, shroud in blue, blade in grey

Figure 11 shows the attached cavity on the pressure side of the blade. Its size is compared to the mean distribution obtained from grey level averaging (Figure 5). Both experimental and numerical NPSH values are equal to 7m. The calculated cavity appears here smaller than the experimental one. Moreover, only the steady attached part of the cavity on the pressure side is obtained by the computation. The transient vapour structures in the unsteady cavity closure are not simulated. Actually this is still a limitation of the physical and numerical model. In this case mesh size and standard turbulence model used do not allow to catch correctly the cloud shedding process downstream from the attached cavity. An ongoing work is pursued to improve this aspect.

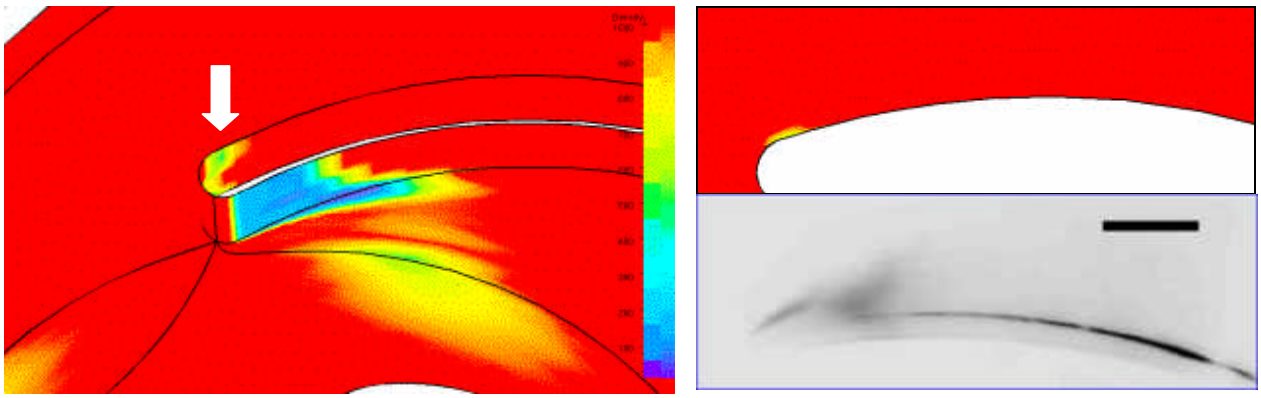

Figure 11: a) Numerical density distribution ; b) pressure side cavity, comparison with experiment (NPSH = 7m).

We summarize in Figure 12 the whole comparison, by drawing the head drop curves for three different flow rates: namely 0.8Qn, Qn and 1.08Qn. From the numerical point of view, while decreasing the NPSH, the performance drop appears first as a smooth decrease of the pump head. The final head-drop is only partially simulated because the computation rapidly becomes unstable and stops (this is more particularly the case at 1.08Qn). Our upstream boundary condition consists in imposing in a strict manner the mass flow rate passing in the pump. Because the coupling between the pump and the hydraulic loop is not taken into account, the effects of the cavitation blockage on the flow rate are neglected and the head-drop is less progressive than in the experiments.
Results obtained from first simulation of the pump cavitation behaviour are promising: the head drop is predicted with a good homogeneity with respect to the three flow rates. The NPSH values obtained for the 3% and 10% head drop are globally overestimated with respect to experimental values (of about 1m for the 10% head drop, and 1.5 to 3 m for the 3% head drop, see Figure 13). These results correspond to our first try of predicting the cavitation characteristic of a pump, and a study of the effect of the model parameters (e.g. the A_{min} value in the state law is set to 2 m/s in that computation or the turbulence model) might probably improve the quantitative agreement.

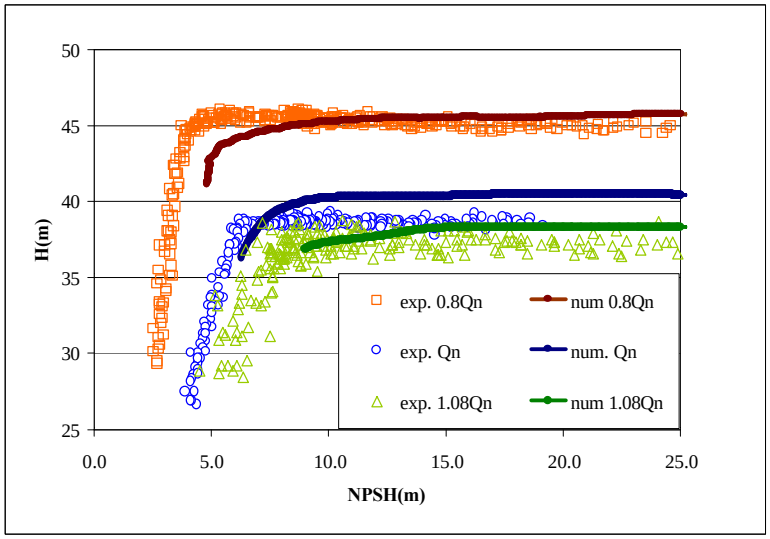

Figure 12. Head-drop curves:
comparison at 0.8Qn, Qn and 1.08Qn

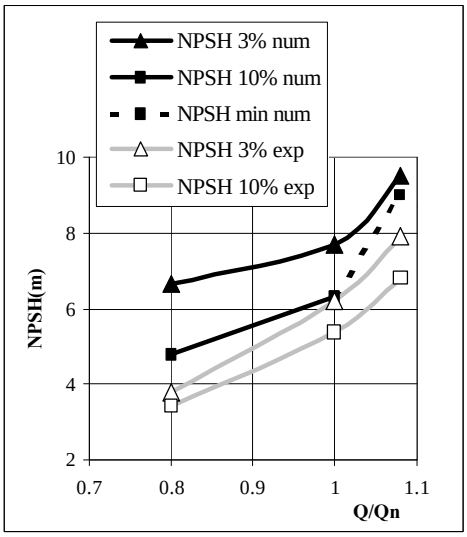

Figure 13: NPSH values
for 3% and 10% head drop.

8. Conclusion

Numerical and experimental results were presented in this study, concerning a test runner with 2D curvature blade geometry. From the experimental point of view, besides the measurements of the cavitation characteristics of the pump in various conditions, a special visualisation set-up was developed to investigate the unsteady behaviour of leading edge cavitation. Image processing and statistical treatment of the photographs taken at given runner position allowed to quantify the attached and cloud cavitation extent.

A numerical model of 3D cavitating flows, based on the 3D code FINE/TURBO^{TM}, has been developed to predict the cavitation behaviour in turbomachinery [Coutier-Delgosha et al. 2001a,b]. This model was applied to the centrifugal pump geometry. Non-cavitating and cavitating conditions were investigated. Calculations were found to be in good agreement with experimental measurements and visualisations. Experimental and numerical results concerning the pump characteristics and performance breakdown were drawn at different flow conditions and the mean spatial distributions of vapour structures within the runner were compared. The results obtained show the ability of the model to simulate the main features of 3D cavitating flows in rotating machinery. However, the fluctuating two-phase areas are not simulated and work is in progress to improve the numerical model in that way.

Acknowledgements

This work is part of a European exchange program PROCOPE with the research teams of Grenoble and Darmstadt as members. The numerical model has been developed with the support of SNECMA Moteurs (Rocket Engine Division), and the French space agency CNES.

References

Alajbevoic A., Grogger H., Philipp H., (1999) *"Calculation of transient cavitation in nozzle using the two-fluid model",* 12th Annual Conf. on Liquid Atomization and Spray Systems, May 16-19, Indianapolis.

Bunnell R.A.and Heister S.D. (2000) *"Three-dimensional unsteady simulation of cavitating flows in injector passages",* J. Fluid Eng. Vol 122, pp 791-797.

Combes JF. et Archer A. (2000) *"Etude de la cavitation dans la pompe SHF",* Coll. Machines Hydrauliques : instationnarités et effets associés, Société Hydrotechnique de France, Chatou, France.

Coutier-Delgosha, O., Fortes-Patella, R., Reboud, J.L., Hakimi, N. (2001a): *"Numerical simulation of cavitating flow in an inducer geometry",* 4th European Conference on Turbomachinery, Firenze, Italy, 20-23 march 2001

Coutier-Delgosha O., Reboud JL., Fortes-Patella R. (2001b): *" numerical study of the effect of the leading edge shape on cavitation around inducer blade sections "*, Proceedings of the 4th Int. Symp. on Cavitation, Pasadena, California, June 2001.

Delannoy, Y., Kueny, J.L. (1990): *"Two phase flow approach in unsteady cavitation modelling"*, Cavitation and Multiphase Flow Forum, ASME-FED vol.98, pp. 153-158

Hakimi, N. (1997): "*Preconditioning methods for time dependent Navier-Stokes equations",* Ph.D.Thesis, Vrije Univ. Brussels.

Hofmann, M. (2001): *" Ein Beitrag zur Verminderung des erosiven Potentials kavitierender Strömungen"* PhD Thesis, TU Darmstadt. to be submitted in June 2001

Hofmann M., Lohrberg H., Ludwig G., Stoffel B., Reboud JL., Fortes-Patella R. (1999): *"Numerical and experimental investigations on the self-oscillating behavior of cloud cavitation: part 1 visualisation / part 2 dynamic pressures"*, 3rd ASME/JSME Joint Fluids Engineering Conference, San Francisco, July 1999

Hofmann M., Stoffel B., Friedrichs J., Kosyna G. (2001): *"Similarities an geometrical effects on rotating cavitation in 2 scaled centrifugal pumps"*, Proceedings of the 4th Int. Symp. on Cavitation, Pasadena, California, June 2001

Kubota A, Kato H., Yamaguchi H. (1992), *A new modelling of cavitating flows: a numerical study of unsteady cavitation on a hydrofoil section*, J. Fluid Mech., vol. 240, pp. 59-96.

Kunz, R., Boger, D., Chyczewski, T., Stinebring, D., Gibeling, H. (1999), "Multi-phase CFD analysis of natural and ventilated cavitation about submerged bodies", 3rd ASME/JSME Joint Fluids Engineering Conference, San Francisco

Lohrberg H., Stoffel B., Fortes-Patella R., Reboud JL. (2001): *"Numerical and Experimental Investigations on the Cavitating Flow in a Cascade of Hydrofoils",* Proceedings of the 4th Int. Symp. on Cavitation, Pasadena, California, June 2001.

Merkle, C.L., Feng, J., Buelow, P.E.O. (1998), *"Computational modeling of the dynamics of sheet cavitation"***,** 3rd Int. Symp. on Cavitation, Grenoble, France.

Reboud J.L., Stutz B. and Coutier O. (1998): *"Two-phase flow structure of cavitation: experiment and modelling of unsteady effects"*, Proceedings of the 3rd Int. Symp. on Cavitation, Grenoble, France, April 1998

Takasugi N., Kato H., Yamagushi H., (1993)*"Study on cavitating flow around a finite span hydrofoil",* Cavitation and Multiphase Flow Forum, ASME-FED vol. 153, pp. 177-182.